Astron. Astrophys. 320, 705–716 (1997)

ASTRONOMY
AND
ASTROPHYSICS

The large scale structure of the soft X-ray background

II. Galaxies

Andrzej M. Sołtan[1,2], **Günther Hasinger**[3], **Roland Egger**[2], **Steve Snowden**[2,4,5], **and Joachim Trümper**[2]

[1] Copernicus Astronomical Center, Bartycka 18, PL-00716 Warsaw, Poland
[2] Max Planck Institut für extraterrestrische Physik, D-85748 Garching, Germany
[3] Astrophysikalisches Institut, D-14482 Potsdam, Germany
[4] NASA/GSFC, LHEA Code 666, Greenbelt, MD 20771, USA
[5] Universities Space Research Association

Received 11 June 1996 / Accepted 12 September 1996

Abstract. The intensity of the soft X-ray background is correlated with the distribution of galaxies. To demonstrate this, magnitude limited galaxy samples extracted from bright galaxy catalogues and the Lick counts are utilized. Significant correlations are detected for all magnitude ranges, i.e. $10 < m_{\rm B} \lesssim 18.6$. The local X-ray volume emissivity between 0.5 and 2.0 keV correlated spatially with the galaxy population falls in the range $(8 \times 10^{38} - 1 \times 10^{39})$ erg s^{-1} Mpc^{-3} ($H_\circ$ = 100 km s^{-1} Mpc^{-1}). Without evolution, this could account for 30 % – 40 % of the total X-ray background, an amount consistent with analogous estimates based on X-ray experiments at higher energies. The comparison of correlation amplitudes of the X-ray background with galaxies at different apparent magnitudes indicates that roughly half of the emission correlated with galaxies can be produced in extended regions substantially larger than optical extent of a typical galaxy. A crude estimate for the average size of these sources is $\sim$ 1 Mpc. This extended signal in various correlation functions is possibly produced by X-ray emission of hot gas in clusters or groups of galaxies, although a contribution from individual galaxies cannot be ruled out.

Key words: cosmology: observations, diffuse radiation – X-rays: galaxies – X-rays: general

1. Introduction

At least 60 % of the soft extragalactic X-ray background (XRB) has been resolved into discrete sources (Hasinger et al. 1993). Thus, the very nature of the XRB is now essentially understood. Apart from optical identificatons and the determination of lumnosity functions of the contributors to the XRB, many current investigations now concentrate on more subtle properties, such as surface brightness fluctuations at various angular scales. Below $\sim 1'$ the inhomogeneity of the XRB is directly related to individual sources. An investigation of the statistical character of these fluctuations shows that at least another 15 % of the total XRB is produced by discrete sources (e.g. Hasinger et al. 1993). At intermediate scales, $1'$ to $\sim 30'$, deviations from a smooth distribution are generated primarily by rich clusters of galaxies (e.g. Briel & Henry 1993, and references therein). Fluctuations at these angular scales could potentially also result from the nonuniform distribution of sources contributing to the XRB. Upper limits on the amplitude of the XRB variations which impose significant constraints on the clustering properties of sources have been obtained by several authors (e.g. Sołtan & Hasinger 1994, and references therein).

At still larger scales, $\theta \gtrsim 0\overset{\circ}{.}5$, low amplitude inhomogeneities could originate from extended nearby sources and/or from sources substantially larger than typical rich clusters. The structure of the XRB at scales above $0\overset{\circ}{.}5$ has been investigated in the first paper of this series (Sołtan et al. 1996, hereafter Paper I). In that work we have measured total fluctuations of the XRB using the auto-correlation function (ACF) of the *ROSAT* All-Sky Survey (RASS) maps (see below). A positive ACF amplitude has been detected for separations up to $\theta \lesssim 6^\circ$. The measurement of the cross-correlation function between the XRB maps and the distribution of Abell clusters revealed that about $1/3$ of the ACF amplitude of the XRB at separations $\lesssim 4^\circ$ can be accounted for by a new class of X-ray emitters associated with rich clusters of galaxies. The origin of the remaining XRB fluctuations is at present unknown. It has been suggested that nearby poor groups of galaxies could potentially contribute to the XRB fluctuations (Hasinger 1992).

This is a second paper of the series which presents further results of our study of the large scale fluctuations of the soft XRB. The aim of this investigation is to determine the average X-ray emissivity of normal galaxies using the extensive RASS data. The X-ray properties of a large number of nearby individual galaxies have been examined on many occasions (e.g. Fabbiano 1989, Eskride et al. 1995, and references therein), but this type of observation cannot be effectively used to determine the total

Send offprint requests to: A. M. Sołtan, Copernicus Center address

local volume emissivity associated with the overall galaxy population. The main thrust of the present investigation is to utilize correlations between distributions of galaxies and the RASS maps. This was recognized as a potential method for studying the XRB several years ago by Turner & Geller (1980). They obtained an upper limit of $\sim 50\,\%$ on the fraction of the XRB in the *Uhuru* energy band ($2 - 6\,\mathrm{keV}$) produced by any class of sources "represented among bright ($m_{pg} \leq 15.5$) galaxies". Jahoda et al. (1991, 1992) calculated the cross-correlation function (CCF) between the *HEAO-1* A-2 all-sky survey ($2-10\,\mathrm{keV}$) and the galaxy surface density based on samples from the Uppsala General Catalogue (Nilson 1973, hereafter UGC) and the European Southern Observatory catalog (Lauberts 1982). The detection of a positive correlation signal led Jahoda et al. to the conclusion that non-evolving sources can produce as much as $50\,\% \pm 30\,\%$ and $70\,\% \pm 40\,\%$ of the XRB respectively, using the two galaxy catalogues. Their figures were revised downward to $(30 \pm 15)\,\%$ by Lahav et al. (1993) who analysed the cross-correlation of the *Ginga* data with the UGC and IRAS galaxy samples. The reason for this reduction resides in different assumptions about the spatial distribution of galaxies contributing to the XRB. Jahoda et al. did not take into account the clustering of galaxies and thus overestimated the average ratio of X-ray emissivity to the surface density of galaxies. Lahav et al. have shown that clustering effects are essential in this case.

A further refinement of this method was achieved by Miyaji et al. (1994), who investigated the cross-correlation between *HEAO 1* A-2 XRB maps and samples of galaxies selected from the *IRAS* point source catalogue. To model the CCF of the XRB – galaxy distribution, they derive formulae describing clustering effects and correlations of X-ray and IR luminosities of the sources under examination. Miyaji et al. point out that their estimates of the total X-ray volume emissivity above 2 keV are model-dependent. Analogous calculations have been performed by Carrera et al. (1995) using *Ginga* scans in the $4-12\,\mathrm{keV}$ band. They found that $\lesssim 10 - 30\,\%$ of the XRB could be produced by a non-evolving population of galaxies.

The angular resolution of both the *HEAO 1* A-2 and *Ginga* LAC experiments is defined by the collimator sizes, $1\overset{\circ}{.}5 \times 3^\circ$ and $1^\circ \times 2^\circ$, respectively. All the cosmic signal of correlations on scales $\lesssim 1^\circ$ is hidden behind the strong correlation amplitude generated by the poor instrumental angular resolution. Because typical correlations between the XRB and galaxy distributions at scales $\gtrsim 1^\circ$ are very weak (see below), investigations based on non-imaging optics are virtually restricted to zero-lag cross-correlation measurements. For instance, this is illustrated by Fig. 2 of Carrera et al. (1995). The correlations are determined over a wide range of separations, but above $\sim 1^\circ$ any CCF signal is lost in the noise.

Three deep *ROSAT* pointings have been used by Roche et al. (1995) to determine the CCF of the unresolved XRB and faint ($B < 23$) galaxies. The angular resolution of the X-ray telescope allowed for measurements of the CCF amplitude at several separations. Although the scatter between fields is substantial, the mean CCF clearly exhibits an extension exceeding the width of the Point Spread Function. The X-ray emissivity estimated by Roche et al. converted to $H_\circ = 100\,\mathrm{km\,s^{-1}\,Mpc^{-1}}$ amounts to $(10.6 \pm 1.4) \times 10^{38}\,\mathrm{erg\,s^{-1}\,Mpc^{-3}}$ in the $0.5 - 2\,\mathrm{keV}$ band. Treyer & Lahav (1995) applied a correlation formalism to investigate the relationship between the population of faint blue galaxies (B = 18 – 23) and the soft XRB. They carefully reevaluated the Roche et al. results and estimate the comoving volume emissivity at $(6 - 9) \times 10^{38}\,\mathrm{erg\,s^{-1}Mpc^{-3}}$ in the $0.5 - 2.0\,\mathrm{keV}$ band.

Total X-ray emissivity correlated with the galaxy distribution is used to estimate contribution of "normal" objects to the total XRB. Term "normal" is commonly used to the overall galaxy population as distinct from variety of objects showing any form of activity. In the present paper, normal objects are those which in the local Universe follow the distribution of sample galaxies. Our analysis cannot be used to distinguish between various mechanisms of galaxy emission. In particular, "classical" normal galaxy emission due to X-ray binaries and SNRs would produce a similar correlation signal to that generated by nuclear galaxy activity distributed among the population of otherwise "normal" galaxies (e.g. Elvis et al. 1984). One could separate stellar signal from scaled down AGN behaviour if the spatial distributions of both types of galaxies are different. Several investigations (Iovino and Shaver 1988, Kruszewski 1988, Andreani and Cristiani 1992, Mo and Fang 1993) show that a class of powerful AGNs, viz. quasars exhibit in fact stronger clustering than general population of galaxies. However, clustering properties of AGNs at the faint end of the nuclear luminosity function are not known and it is likely that the spatial distribution of these galactic nuclei is identic to the general galaxy distribution.

Identification of X-ray sources directly show what kinds of objects contribute to the XRB at various flux levels. Here we summarize basic data on this subject for comparison with the present results. The largest contribution to the XRB above *ROSAT* sensitivity threshold comes from AGNs (e.g. Boyle et al. 1993 and references therein). The deepest *ROSAT* exposure in the *Lockman Hole* resolves about 60 % of the background with AGNs clearly seen in high proportion (Hasinger et al. 1993, Bower et al. 1996). Systematic identifications of X-ray sources in a large number of *EINSTEIN* and *ROSAT* fields show that QSOs with luminosities in the range $10^{42} - 10^{46}\,\mathrm{erg\,s^{-1}}$ in the soft X-rays produce 30 % to 90 % of the XRB at 2 keV. Although, due to poor estimates in the faint end and high redshift evolution of the X-ray luminosity function, above limits are still wide, it is well established that the AGN contribution to the XRB is substantially larger than the contribution of ordinary galaxies, i.e. galaxies which produce X-rays through standard thermal processes.

Detailed studies of nearby galaxies and the Milky Way reveal a variety of X-ray sources associated with several galaxy components. The total X-ray emission of an individual galaxy is a mixture of several constituents. The integrated flux produced by single and binary stars, supernova remnants, thermal emission by hot gas and – in some objects – non-thermal radiation produced in an active nucleus create a complex X-ray map for each galaxy (e.g. Fabbiano 1989 and references therein).

Observations using the *EINSTEIN* and *ROSAT* satellites show that normal galaxies of all morphological types are spatially extended X-ray sources with luminosities in the range of $\sim 10^{38}$ to $\sim 10^{42}$ erg s^{-1}. Separate from this "normal" X-ray emission, some fraction of galaxies exhibit non-thermal nuclear activity. It is likely that luminosities of active galactic nuclei extend to arbitrary low levels and the distinction between normal and active galaxy could in some cases be a matter of convention (e.g. Elvis et al. 1984). Using ratio of X-ray to optical luminosities (excluding non-thermal nuclear component) integrated emission of normal galaxies contributes $\sim$ 13 % to the XRB at 2 keV (Fabiano 1989).

Clusters of galaxies constitute a separate class of X-ray sources. Observations of distant clusters (e.g. Edge et al. 1990, Henry et al. 1992, Ebeling 1993, but see also Ebeling et al. 1996) indicate – although this question still could be debated – that their X-ray luminosity function undergoes strong evolution in the sense that local volume emissivity is greater than that at high redshifts. According to various estimates, contribution of rich, Abell-type, clusters to the XRB falls between 5 % and 10 %.

Correlations between the XRB and selected galaxies provide information on all kinds of X-ray sources which are spatailly correlated with those galaxies. The CCF signal represents integrated emission of sources occupying specific volume. Luminosity density calculated this way comes both from normal galaxies and AGNs as well as from clusters of galaxies (see below). The present calculations give the X-ray volume emissivity but do not allow to isolate individual objects. On the other hand, identifications of sources in flux limited samples provide information on discrete sources, but are ineffective method to calculate total volume emissivity.

In this context it is important to note that our samples were constructed using apparent magnitudes. Any X-ray emission which is not correlated with galaxies (e.g. hypothetical X-ray sources associated with dwarf galaxies in voids) is not taken into account. Thus our measurement is actually a lower limit for the total X-ray emissivity if other kinds of X-ray sources are common in the local Universe.

The basic framework of the present investigation is analogous to the work by Roche et al. (1995), although we are using totally different observational material both in the X-ray and optical domains. The main advantage of the present analysis resides in the high quality of the X-ray data accumulated in the RASS. The massive amount of the RASS data warrants not just a quantitative improvement of the measurement accuracy, but also a substantial extension of the scope of analysis as compared to the previous investigations. Our objective is to determine the CCFs between the XRB and several magnitude limited galaxy samples. These observed CCFs are compared with predictions based on the correlations of galaxies measured in each sample separately and between the samples. Then, we estimate the ratio of the X-ray–to–optical volume emissivities associated with galaxies and – using optical luminosity density as normalization – we calculate the X-ray volume emissivity. The organization of the paper is as follows: the X-ray and optical material used in the investigations is described in Sects. 2 and 3, respectively. Procedures used to determine the CCFs and their uncertainties are presented in Sect. 4. An analysis of the observed CCFs and the construction of models which properly reproduce the observations is given in the Sect. 5. We examine some properties of the X-ray emission in Sect. 6 and conclude our investigation with a short discussion in Sect. 7.

2. Selection of the X-ray data

The *ROSAT* (Trümper 1983) All-Sky Survey with the PSPC (Pfeffermann et al. 1986) is used in the analysis. For a comprehensive description of the RASS see Snowden & Schmitt (1990) and Voges (1992). Basic references and relevant characteristics of the RASS are given in Paper I. Here we summarize only the essential information. Various effects and constituents contaminating the cosmic signal (particle background, solar scattered X-rays and "short- and long-term enhancements") have been extracted in a complex and laborious procedure as described by Snowden et al. (1995). Within the *ROSAT* energy band (0.1 − 2.4 keV), the amplitude of the galactic component relative to the extragalactic signal increases drastically towards soft energies. In Paper I we discuss this question in some detail and find that useful information on the fluctuations of the extragalactic XRB component are concentrated mainly in two energy bands in the hard portion of the RASS labelled R5 and R6. The band R5 is centered at $\sim$ 0.8 keV and in terms of puls-height invariant (PI) channels includes channels $70 - 90$, while the band R6 is defined by channels $91 - 131$ and is centered at $\sim$ 1.1 keV (Snowden et al. 1994b). Although the bands R5 and R6 cover overlapping energy ranges, they differ strongly in the level of the galactic contribution. It is shown in Paper I that a specific linear combination of the count rates in bands R6 and R5 is significantly less contaminated by soft emission from hot plasma in the Galaxy than each of those bands separately. Because in the present investigation we are interested in the extragalactic component of the XRB, we use exactly the same procedure as in Paper I to obtain data free from the local contamination, viz. we utilize a region in the North Galactic Hemisphere:

$$70^\circ < l < 250^\circ, \quad b > 40^\circ, \tag{1}$$

in which the count rate of the extragalactic component in the band R6, CR^{ext}_{R6}, is defined as

$$CR^{ext}_{R6} = 1.15\, CR_{R6} - 0.23\, CR_{R5}, \tag{2}$$

where CR_{R5} and CR_{R6} denote the count rates in the respective bands (see Paper I for details).

For the purpose of the present paper, the RASS maps are represented by an array of count rates in pixels. Pixels of $12' \times 12'$ are used in our calculation. This size coincides roughly with the area containing 90 % of the counts produced by a point source.

3. Optical data – galaxy distribution

Galaxy data were divided into several magnitude limited samples. To construct maps of the galaxy distribution suitable for

Table 1. Galaxy sample parameters

Sample	Mag range	ρ [pxl^{-1}]	$z_{\rm mean}$
1	10 – 12	1.26×10^{-3}	0.004
2	12 – 14	6.60×10^{-3}	0.010
3	14 – 15	1.80×10^{-2}	0.018
4	15 – 16	6.05×10^{-2}	0.024
5	16 – 18.6	1.730	0.062

further analysis, we have used the *Catalogue of Principal Galaxies*, hereinafter, PGC described by Paturel et al. (1989) and Shane and Wirtanen (1967, hereafter SW) counts in $10'$ pixels kindly provided to us in electronic form by Dr. M. Kurtz. Galaxies selected from the PGC are divided into four samples according to apparent magnitude limits: sample 1 contains galaxies with $10 < m < 12$, sample 2 with $12 < m < 14$, sample 3 with $14 < m < 15$ and sample 4 with $15 < m < 16$. The first three samples are statistically complete, while in sample 4 some galaxies at the faint magnitude limit are missing due to the incompleteness of the PGC (see below). The fifth sample contains galaxies from the SW counts excluding those present in the first four samples. Thus, it comprises the weakest and – on the average – the most distant galaxies.

To assess completeness of sample 4, we have used the slope of the number–magnitude relation. In the relevant magnitude range it is approximately equal to 0.55 (Driver et al. 1994), which is slightly below the slope expected in the Euclidean non-expanding model of 0.6. The number of galaxies expected in sample 4, based on the extrapolation from samples 2 and 3 and a slope of 0.55, is 6 % larger than that actually listed. Using the Euclidean slope of 0.6, this difference increases to 23 %.

The average number of galaxies in $12' \times 12'$ pixel in the sample 5 is 1.730. We derive the approximate faint magnitude limit in this sample of 18.6 mag, using the bright end limit of 16 mag and assuming the slope of the relation between number counts and apparent magnitude ≈ 0.5 (Driver et al. 1994). A summary of the relevant data on the galaxy samples is given in Table 1.

In the last column of Table 1 we list the mean galaxy redshift in each sample. For samples 1 through 4 $z_{\rm mean}$ denotes the average value calculated for galaxies with known redshifts. In sample 1 all galaxies but one have measured redshift. The fraction of such galaxies in samples 2, 3 and 4 drops to 0.91, 0.55 and 0.14, respectively. The $z_{\rm mean}$ in sample 5 is obtained from the model calculations in Sect. 5.2.

4. Cross-correlation of X-ray maps with galaxy distributions

The wide range of X-ray luminosities of galaxies and the heterogeneity of spatial structures and emission mechanisms complicate estimates of average sample properties. The RASS offers a possibility to measure the overall galaxy emission using a large sample of galaxies. Obviously, the angular resolution and sensitivity of the RASS is not adequate to study weak objects individually. The typical signal-to-noise ratio for the X-ray detection of galaxies is usually less than one and most galaxies cannot be recognized as distinct sources. Nevertheless, X-ray fluctuations produced even by the most distant galaxies in our samples (see below) are easily measured using the correlation technique. This allows us to measure the average X-ray emission associated with the overall galaxy population.

Rich galaxy clusters constitute a well established and recognized class of sources in which the X-ray emission originates in the hot intracluster gas and is not linked with individual galaxies. With the exception of the few brightest clusters, the flux produced in individual galaxies cannot be separated from the cluster emission in the RASS maps. Thus, the question of the cluster contribution to the local luminosity density associated with galaxies could not be addressed in the present investigation. Furthermore, the distribution of galaxies is correlated with the distribution of rich clusters of galaxies over a wide range in separation (Seldner & Peebles 1977). This correlation also affects our present analysis. The effects produced by Abell clusters are measured directly in Sect. 4.2 where we obtain the CCFs of the RASS maps and galaxy samples using two sets of data. In the first case, the full observational material including Abell clusters is utilized. Then we remove from the data areas containing Abell clusters and repeat the CCF calculations.

The contribution of clusters and groups not included in the Abell catalogue is discussed in the Sect. 6.

4.1. Definitions

The CCF is defined in a standard way:

$$w_{Xg}(\theta) = \frac{\langle \rho_X(\mathbf{n}) \rho_g(\mathbf{n}') \rangle_\theta}{\langle \rho_X \rangle \langle \rho_g \rangle} - 1, \tag{3}$$

where $\rho_X(\mathbf{n})$ is the intensity of the X-ray background in the direction $\mathbf{n}$ and $\rho_g(\mathbf{n}')$ is the surface density of galaxies in the direction $\mathbf{n}'$, $\langle ... \rangle$ denote the expectation values and θ is the angle between $\mathbf{n}$ and $\mathbf{n}'$. The distribution of galaxies in samples 1 – 4 is binned into pixels exactly the same as those used for the X-ray maps. Galaxies in sample 5 have also been organized into the present pixels, although it required regrouping the galaxies from the original 10 arc min pixels. Galaxies in the SW pixel have been redistributed into new ones proportionally to the overlapping pixel areas. This procedure effectively smoothed out the original data over a scale comparable to the pixel size. The binned galaxy data form arrays analogous to the X-ray count rate distributions, where $\rho_g(i)$ is equal to 0, 1, 2,.. according to the number of galaxies found in the i-th pixel. To estimate $w_{Xg}(\theta)$ the expectation values in Eq. (1) are substituted by their respective averages obtained from the data:

$$W_{Xg}(\theta) = \frac{\frac{1}{n_{ij}(\theta)} \sum_{ij} \rho_X(i) \rho_g(j)}{\overline{\rho_X}\ \overline{\rho_g}} - 1, \tag{4}$$

where $\rho_X(i)$ is the count rate in the i-th pixel and the sum extends over all pixel pairs with centers separated ($\theta - 6$ arc min) and ($\theta + 6$ arc min); n_{ij} is the number of such pairs in the data and $\overline{\rho_X}$ and $\overline{\rho_g}$ are the average X-ray count rate and galaxy density, respectively.

4.2. Numerical results

Correlations between the X-ray distribution and all galaxy samples listed in Table 1 have been computed and the results are shown in Fig.1. Open squares refer to samples selected from the PGC (samples 1 through 4) and filled small squares to galaxies from the SW counts. The size of the symbols corresponds to the apparent magnitude of galaxies in the sample: the largest squares represent sample 1, the smallest – sample 4. The CCF points at the lowest separation give the zero-lag correlations, i.e. $i = j$ in Eq. 4. All the CCFs shown with squares refer to data which do not contain the Abell clusters. Pixels close to the position of all Abell clusters have been removed from the RASS maps and the galaxy samples. The size of the removed areas has been scaled with the cluster distance class (DC). For the most distant clusters (DC = 5 and 6), the pixel containing the cluster and 8 surrounding pixels have been deleted. For DC = 3 and 4 a radius of 2 pixels was used and for DC = 2 and 1 the areas with radius of 3 and 4 pixels, respectively, were excluded. Crosses in Fig.1 represent the CCF of the sample 5 using all the data, i.e. including Abell clusters. The effect produced by Abell clusters is pronounced over a wide range of separations: the ratio of the CCF amplitude calculated without clusters to that using all the data amounts to ~ 0.6 and is roughly constant for $\theta < 10^\circ$. Sample 4 is less affected by Abell clusters and the ratio of ACF amplitudes reaches 0.8. Galaxies in samples 1, 2 and 3 are virtually not correlated with Abell clusters and the relevant CCFs do not differ significantly. The strong contribution of Abell clusters to the galaxy–XRB correlations accentuates the cluster contribution to the local luminosity density correlated with the galaxy population. To reduce the cluster signal in the subsequent analysis we use the data without Abell clusters. Since the Abell catalogue is not statistically complete and many smaller galaxy groups are also X-ray emitters, the excision of just the Abell clusters removes a fraction of X-ray emission produced by intracluster gas from the RASS maps. In effect, we are unable to eliminate completely clusters from our analysis and the signal in the respective CCFs represents the sum of both contributions.

Some scatter resulting from statistical fluctuations is visible, particularly in sample 1 which contains only 108 galaxies. Despite this scatter, there are conspicuous systematic trends. The shapes of all CCFs are similar over a wide range of separations. Below $\sim 1^\circ$ the CCF amplitudes decrease uniformly, while between 1° and 10° all the CCFs exhibit some flattening. At the smallest separations ($\theta < 0.^\circ 3$), where the signal-to-noise ratio is high, the CCF amplitudes decrease systematically from sample 1 to 5. Substantial errors at larger separations make this trend less apparent but it is still visible. The uncertainties of our CCF measurements are difficult to determine. The nonuniform distribution of galaxies on the celestial sphere combined with relatively high fluctuations of the XRB on scales up to several degrees generate quite large uncertainties of the correlation functions. One should point out that actual CCF uncertainties are significantly larger than those expected from the rms X-ray count rate scatter and random distribution of galaxies. We discuss this question in Paper I and find that reasonable estimates

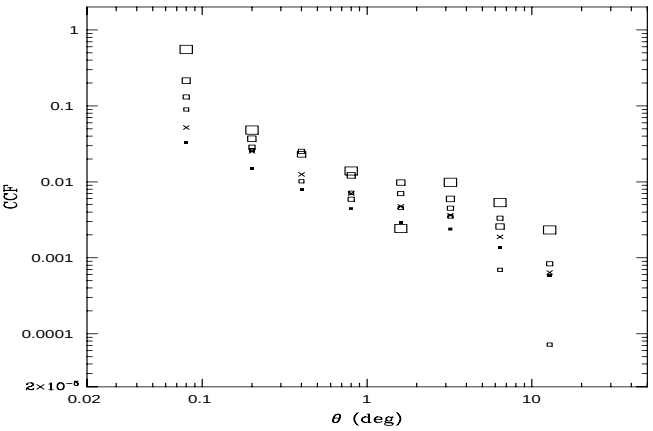

Fig. 1. The raw cross-correlation functions (CCFs) of five galaxy samples and the RASS X-ray maps. Open squares denote four samples from the PGC, filled squares the SW galaxy counts (sample 5). The size of the open symbols corresponds to the apparent magnitude of galaxies: largest squares – sample 1, smallest squares – 4 (see Table 1). The CCFs shown with squares represent the data without the Abell clusters, crosses show the CCF of the SW and RASS data including Abell clusters

of total errors could be obtained by means of simulations. Several randomized CCFs are generated using the original X-ray data and galaxy maps rotated around the galactic polar axis. This method removes correlations between the data but does not affect the statistical properties of each distribution. The amplitudes of simulated CCFs are produced just by random coincidences of fluctuations in both data sets. It is postulated that the rms scatter between simulations represents total uncertainties of the CCF estimates. We note, however, that the average simulated CCFs are systematically positive, while one should expect symmetric fluctuations around zero. Because a rotation of the galaxy data around the galactic polar axis does not eliminate a dependence of the galaxy distribution on the galactic latitude, positive amplitudes of simulated CCFs suggest that there is also some systematic trend of the X-ray data with galactic latitude. To correct for this effect, we have subtracted from the observed correlations the average simulated amplitudes in each sample. At small separations the extragalactic signal dominates and the correction is small, but above $\sim 1^\circ$ the galactic contamination is non-negligible. Results for 5 samples are shown in Figs. 2 a–e (where the symbols refer to the same samples as in Fig. 1). Error bars correspond to the rms scatter between simulations. In sample 5 the net correlation extends clearly to several degrees. For nearby samples with relatively small number of galaxies uncertainties are comparable to the signal on scales above $\sim 1^\circ$.

5. Galaxy distribution vs. the X-ray background fluctuations

The CCFs obtained in the previous section describe the coupling between the galaxy distribution and the intensity of the X-ray background radiation. The amplitude $W_{Xg}(\theta)$ gives the relative enhancement of the X-ray intensity at separation θ of a randomly

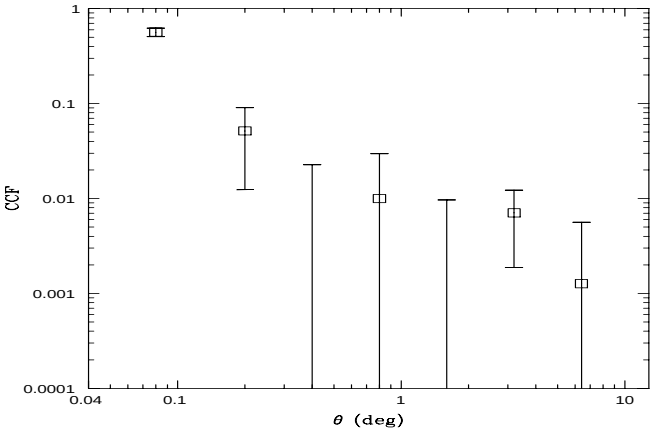

Fig. 2a. The net CCF (viz. raw CCF – simulated CCF) of the PGC sample 1 and the RASS map. Error bars represent rms in the simulations

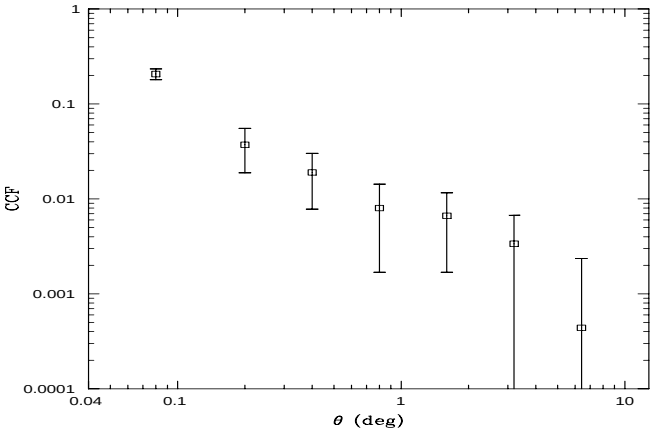

Fig. 2b. Same as Fig. 2a for sample 2

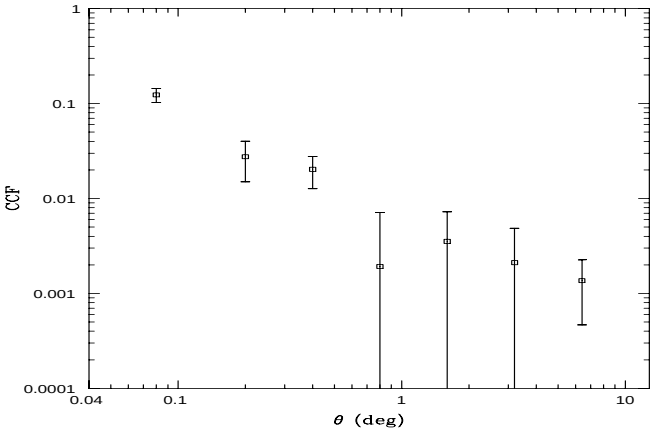

Fig. 2c. Same as Fig. 2a for sample 3

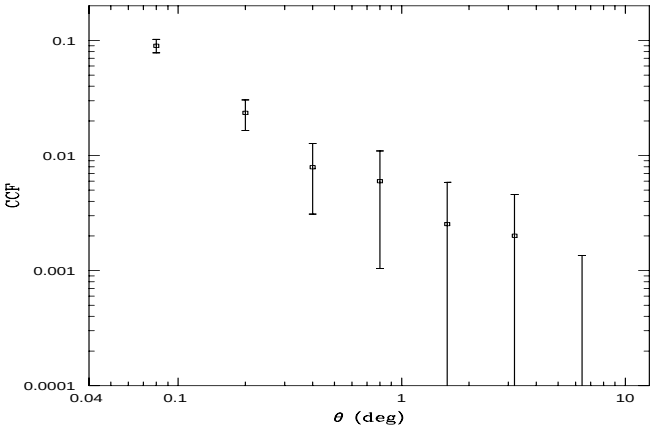

Fig. 2d. Same as Fig. 2a for sample 4

chosen galaxy. At small separations, particularly for zero-lag, this enhancement is produced mostly by the individual galaxy itself, while at larger distances the signal results from other X-ray sources which are correlated with galaxies from the sample.

The average distribution of galaxies around a randomly chosen object is described by galaxy correlation functions. Thus, the CCFs between the X-ray data and the galaxy distribution shown on Figs. 2a–e depend on the galaxy–galaxy correlation functions. The formulae of the auto-correlation function of galaxies in a single sample and the cross-correlation function between two galaxy samples are analogous to those given by Eqs. (3) and (4): the ACF of galaxies in the sample k ($k = 1, ..., 5$), $w_{kk}(\theta)$ is defined as follows:

$$w_{kk}(\theta) = \frac{\langle \rho_k(\mathbf{n})\rho_k(\mathbf{n}')\rangle_\theta}{\langle \rho_k\rangle^2} - 1, \tag{5}$$

and the CCF between samples k and l, $w_{kl}(\theta)$:

$$w_{kl}(\theta) = \frac{\langle \rho_k(\mathbf{n})\rho_l(\mathbf{n}')\rangle_\theta}{\langle \rho_k\rangle\langle \rho_l\rangle} - 1. \tag{6}$$

The number of excess galaxies per pixel above the average concentration from sample l at separation θ from a randomly chosen galaxy in sample k is described by the appropriate CCF (e.g. Peebles 1980):

$$n_{kl} = \langle \rho_l\rangle \cdot w_{kl}(\theta). \tag{7}$$

Let f_l^{opt} denote the average optical flux produced by a galaxy from the sample l. Then the total enhancement of the optical surface brightness of the sky around a randomly chosen galaxy in the sample k, Δf_k^{opt}, due to galaxies in all the samples is given by:

$$\Delta f_k^{opt}(\theta) = A_k^{opt}(\theta) + \sum_l f_l^{opt}\langle \rho_l\rangle w_{kl}(\theta), \tag{8}$$

where term $A_k^{opt}(\theta)$ accounts for the finite size of galaxies and denotes the average optical flux produced by the chosen galaxy in a pixel at a separation θ and the sum extends over all galaxy samples which exhibit correlations with the sample k.

The CCF between galaxies in sample k and the X-ray distribution gives the average excess of the X-ray intensity around a randomly chosen galaxy:

$$\Delta f_k^X(\theta) = \langle \rho_X\rangle w_{Xk}(\theta). \tag{9}$$

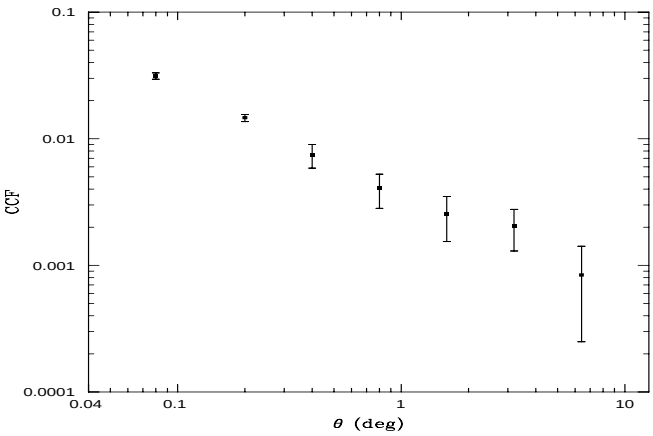

Fig. 2e. Same as Fig. 2a for sample 5

The ratio of fluctuation amplitudes in both domains (X-ray and optical) defined by Eqs. (8) and (9) is used to determine the galaxy contribution to the XRB in the next section.

5.1. Approximate solution

We define the optical flux by means of B magnitudes as:

$$f^{opt} = \nu_B \, f_{\nu_B} \tag{10}$$

where $\nu_B = 6.8 \times 10^{14}$ Hz is the effective frequency of the B band[1]. We have used the following conversion from the B band to energy flux f_{ν_B} in erg s^{-1} cm^{-2} Hz^{-1}: $\log f_B = -19.41 - 0.4\,\mathrm{B}$ (Butcher et al. 1980). Note, that the zero point of this normalization as well as the particular definition of f^{opt} in Eq. 10 do not affect our subsequent estimates of the galaxy contribution to the XRB. This is because in the calculations we utilize effectively the ratio of X-ray to optical fluxes and the ratio of corresponding absolute luminosities. It requires, however, consistent definitions of optical apparent flux and absolute luminosity in the B band (see Eq. 12).

Because our galaxy data collected in five samples cover an apparent magnitude range between 10 and $\sim$ 18.6, Eq. (8) for each $k = 1, ..., 5$ describes only the fraction of optical fluctuations which is associated with galaxies in these samples. The bright magnitude constraint of 10 is not restrictive because the small number of galaxies with $m < 10$ does not affect the observed correlations. The problem of galaxies not included in the calculations is severe at the faint end. Numerous galaxies below the SW count threshold influence the observed CCFs. The effect is strongest for sample 5, but could also be important for other samples. In the first approximation we ignore all the cross-correlation terms in Eq. (8) and use only the ACFs. We avoid problems with the point response function and calculations of A_k by using the CCFs integrated over separations $\theta < 18'$, a distance significantly larger than the effective angular resolution of the RASS. In this case, $A_k(\theta)$ is replaced by f_k^{opt} and Eqs. (8) can be rewritten in the form:

$$\Delta f_k^{opt}(\theta) = \sum_l f_l^{opt}(\langle \rho_l \rangle W_{kl} + \delta_{kl}), \tag{11}$$

where W_{kl} denotes the CCF estimator defined by Eq. (4), $\delta_{kl} = 1$ for $l = k$ and $\delta_{kl} = 0$ otherwise. Amplitudes W_{kl} are calculated using overlapping pixels (zero lag) and the nearest neighbours (first two points on Figs. 2a-e).

The average count rate defined by Eq. (2) in the discussed area $\langle \rho_X \rangle = 74.6 \times 10^{-6}$ PSPC cnt s^{-1} arcmin^{-2}. Conversion rates of PSPC counts to the flux units are given for various spectra in Paper I. In the following calculations we adopt a conversion factor corresponding to a power law spectrum with an energy spectral index of -1 and a hydrogen column density of 1.8×10^{20} cm^{-2}, as these parameters are representative for our energy band and sky region (Hasinger 1992, Paper I). Using the standard calibration of the PSPC we find that 1 PSPC cnt s^{-1} is equivalent to a flux outside the Galaxy of 3.29×10^{-11} erg cm^{-2} s^{-1} in the 0.5 - 2.0 keV energy band.

The fluctuation amplitudes in the X-ray band obtained using Eq. (9) with the W_{Xk} estimators defined by Eq. (4) are given in column 2 of Table 2. Fluctuations in the optical domain produced by galaxies in the sample under consideration are calculated by means of Eq. (11) using only the auto-correlation term i.e. $k = l$ are denoted by Δf_k^{opt}(ACF) and are given in column 3. The optical data quoted in Table 2 ignore the nonuniform distribution of galaxies in other samples and underestimate the actual optical fluctuations. In column 4 the ratio of X-ray to B-band fluctuations $R_k^{ACF} = \Delta f_k^X / \Delta f_k^{opt}$(ACF) is listed. Systematic variations of R_k^{ACF} by a factor of $\sim$ 12 indicate that the CCF terms in Eq. (11) are significant. A signal-to-noise ratio of the galaxy–X-ray CCF determinations used to compute Δf_k^X is listed in column 5.

Table 2. X-ray and optical fluxes (approximate solution)

Sample k	Δf_k^X [erg s^{-1} cm^{-2}]	Δf_k^{opt}(ACF)	$\Delta f_k^X / \Delta f_k^{opt}$(ACF)	S/N
1	3.45×10^{-13}	8.74×10^{-10}	0.00040	1.23
2	1.78×10^{-13}	1.61×10^{-10}	0.0011	2.02
3	1.22×10^{-13}	4.92×10^{-11}	0.0025	2.20
4	9.83×10^{-14}	2.61×10^{-11}	0.0038	3.36
5	5.23×10^{-14}	1.05×10^{-11}	0.0050	15.5

5.2. Model galaxy distribution

The distributions of galaxies in the different magnitude ranges are highly correlated. This is because the galaxy luminosity function extends over several magnitudes and galaxies occupying the same volume of space can be members of various magnitude limited samples. Also, the apparent magnitudes of galaxies listed in the PGC are subject to fairly large errors which additionally spread spatially intermingled galaxies over different samples. Cross-correlations between samples increase the

[1] Note that flux in the optical domain in various papers is defined differently, e.g. Maccacaro et al. (1988) define the optical flux as: $\log f_v = -0.4 m_v - 5.37$ while our Eq. (10) is equivalent to $\log f^{opt} = -0.4 m_B - 4.57$.

Table 3. The ACF amplitudes averaged over $36' \times 36'$

Sample	W_{kk} - observed	w_{kk} - model
1	5.76	5.55
2	3.79	3.66
3	1.48	1.96
4	1.04	1.06
5	0.23	0.26

total fluctuation amplitude of the optical light substantially. Using the CCFs between our 5 galaxy samples we can directly measure fluctuations associated with galaxies brighter than B $\approx$ 18.6. Effects produced by fainter galaxies are estimated using the model distribution of galaxies.

Estimates of the angular correlation amplitudes of galaxies in the magnitude limited samples are obtained assuming standard 3D galaxy correlation function in the form: $\xi(r) = (r/r_\circ)^{-\gamma}$. It has been assumed that $\xi(r)$ is independent of the absolute luminosity of galaxies. We have used flat cosmological model with $H_\circ = 100\,\mathrm{km\,s^{-1}Mpc^{-1}}$, $\Lambda = 0$ and $q_\circ = 0.5$. To generate the redshift distribution of galaxies at given apparent magnitude and subsequently, to calculate the galaxy angular correlation functions, the galaxy luminosity function (LF) is needed. In the calculations the LF has been approximated by the Schechter (1976) function with $\mathrm{M_B^*} = -19.49$ and $\alpha = -1.5$. Driver et al. (1994) discussed various models of the galaxy luminosity distributions consistent with the galaxy counts. Parameters used in the present paper are adopted from the Driver et al. model based on a single Schechter function. We have also used their approximations for K-corrections. Even with such simplified model we have been able to reproduce fairly well the ACF amplitudes measured in our galaxy samples. To fit the predicted amplitudes to the observed ones we varied only the spatial correlation length $r_\circ$ and the best agreement has been found for $r_\circ = 4.0\,\mathrm{Mpc}$. In Table 3 we compare the observed and calculated ACF amplitudes averaged over 9 pixels.

Using the present model we have calculated the CCFs between the galaxy samples 1 – 5 and galaxies fainter than $\mathrm{m_B} = 18.6$. In the computations we have divided the latter galaxies into 5 magnitude bins with $\Delta\mathrm{m_B} = 1$: 18.6 – 19.6 – ... – 22.6 – 23.6. Substituting the actual CCF amplitudes W_{kl} for $k, l = 1, ..., 5$ and model amplitudes for $k = 1, ..., 5$ and $l = 6, ..., 10$ into Eq. (11) we calculated the average fluctuations of the sky brightness in the B band around sample galaxies down to $\mathrm{m_B} = 23.6$. Effects produced by fainter galaxies were estimated using extrapolation from $\mathrm{m_B} < 23.6$. Contributions of $\mathrm{m_B} > 23.6$ galaxies relative to those brighter than 23.6 are below 1 % for fluctuations around galaxies in three brightest galaxy samples (k = 1, 2, 3) and reach 1.6 % and 4.9 % for samples 4 and 5, respectively. Results of these calculations are given in Table 4.

Observed average amplitudes of optical fluctuations produced by galaxies brighter than $\mathrm{m_B} = 18.6$ are listed in column 2. Estimates of total fluctuations Δf_k^{opt}(total) and X-ray–to–optical ratios $R_k^{tot} = \Delta f_k^X / \Delta f_k^{opt}$(total) are given in columns 3 and 4, respectively. We note that R_k^{tot} exhibits still large variations, although it is substantially more stable than R_k^{ACF}. We discuss variations of R_k^{tot} in the next section.

The ratio of apparent fluctuations R_k^{tot} is equal to the ratio of X-ray–to–optical volume emissivities $\mathscr{L}_X / \mathscr{L}_{opt}$. We calculate the optical volume emissivity in the B-band integrating the LF over all the optical luminosities:

$$\mathscr{L}_{opt} = \nu_\mathrm{B} \int L_{\nu_\mathrm{B}}\, \varphi(L_{\nu_\mathrm{B}})\, dL_{\nu_\mathrm{B}} = n^*\, \nu_\mathrm{B}\, L^*_{\nu_\mathrm{B}}\, \Gamma(\alpha + 2)$$
$$= 5.20 \times 10^{41}\,\mathrm{erg\,s^{-1}\,Mpc^{-3}}, \quad (12)$$

where $n^* = 1.47 \times 10^{-2}\,\mathrm{Mpc^{-3}}$ is the normalization of the Schechter LF, $L^*_{\nu_\mathrm{B}} = 2.92 \times 10^{28}\ \mathrm{erg\,s^{-1}Hz^{-1}}$ corresponds to $\mathrm{M_B^*} = -19.49$. The galaxy counts using these parameters are in good agreement with the actual number of galaxies in our samples. We now calculate the X-ray volume emissivity $\mathscr{L}_X(gal)_k$ correlated with the galaxy distribution for each sample:

$$\mathscr{L}_X(gal)_k = R_k^{tot}\, \mathscr{L}_{opt}. \quad (13)$$

To assess contribution of this local emission to the total XRB, we note that without cosmological evolution $\mathscr{L}_X(total) = 2.73 \times 10^{39}\,\mathrm{erg\,s^{-1}\,Mpc^{-3}}$ in the 0.5 – 2.0 keV band is required to produce the observed intensity of the XRB (Hasinger et al. 1993, Paper I). In column 5 of Table 4 we list the ratio:

$$C_k = \mathscr{L}_X(gal)_k / \mathscr{L}_X(total), \quad (14)$$

Thus, C_k denotes the fractional contribution to the XRB by a nonevolving population of sources generating a constant luminosity $\mathscr{L}_X(gal)_k$ per unit volume of co-moving space integrated to large redshifts (e.g. Paper I, Eq. 18).

Estimates of the local volume X-ray emissivity and its contribution to the XRB based on 5 galaxy samples still cover an uncomfortably wide range. Albeit this is distinctly smaller than variations of R_k^{ACF} found when the cross-correlation terms were ignored (column 4 in Table 2), present C_k measurements span from 7 % to 38 %. These changes are inconsistent with one value, expected if X-ray properties of each sample are representative to the whole galaxy population. Growth of C_k with k taken literally would indicate that samples have substantially different average X-ray luminosities associated with a single galaxy. Obviously, such interpretation is not accepted and an alternative systematic effect is proposed in the next section to explain sample-to-sample variations.

6. Effects of extended emission

The ratios of X-ray–to–optical fluctuations have been calculated in the preceding section for separations $\theta < 18'$. We now apply these quantities to synthetize predicted CCF between the galaxy distribution and the X-ray sky in the wider range of separations and compare them with the actual measurements. The procedure is as follows. The amplitude of the optical fluctuations $\Delta f_k^{opt}(\theta)$ is calculated by means of Eq. (11) using galaxy ACFs and CCFs $W_{kl}(\theta)$. The "δ_{kl}" term at the right-hand side of the equation is used only for zero lag correlations ($i = j$ in Eq. (4)). Then the values $\Delta f_k^X(\theta)$ are obtained using the R_k^{tot} from column 4

Table 4. Galaxy contribution to the XRB

Sample	$\Delta f_k^{opt}(m_B < 18.6)$	Δf_k^{opt}(total)	$\Delta f_k^X / \Delta f_k^{opt}$(total)	C_k
k	[erg s^{-1} cm^{-2}]			
1	9.22×10^{-10}	9.25×10^{-10}	0.00037	0.071
2	2.18×10^{-11}	2.26×10^{-10}	0.00079	0.15
3	8.69×10^{-11}	9.53×10^{-11}	0.0013	0.24
4	4.81×10^{-11}	5.67×10^{-11}	0.0017	0.33
5	1.67×10^{-11}	2.59×10^{-11}	0.0020	0.38

of Table 4. Finally, predicted CCF $w_{Xk}(\theta)$ for $k = 1, ..., 5$ are calculated from Eq. (9) and the results are shown in Figs. 3a-e. Open squares and error bars show the actual galaxy–X-ray CCF (same as in Figs. 2a-e), while crosses represent calculated CCFs according to above prescription. For comparison, the ACFs in each galaxy sample are shown with filled symbols.

Results for sample 1 (Fig.2a) do not allow to make conclusive statements due to excessive uncertainties. We note only that observed and synthetized ACFs in sample 1 are in qualitative agreement and the subsequent discussion is limited to the samples $k = 2 - 5$. At separations below $18'$ all calculated CCFs exhibit similar deviations from the actual measurements: the synthetized zero-lag point is situated above the real one, while the relative positions of the next point ($6' < \theta < 18'$) are reversed. This is because the predicted galaxy–X-ray CCFs are obtained under the assumption that the galaxy residing in the zero-lag pixel does not produce X-ray signal in the surrounding pixels. This condition is not satisfied in the real CCF due to the finite width of the point spread function.

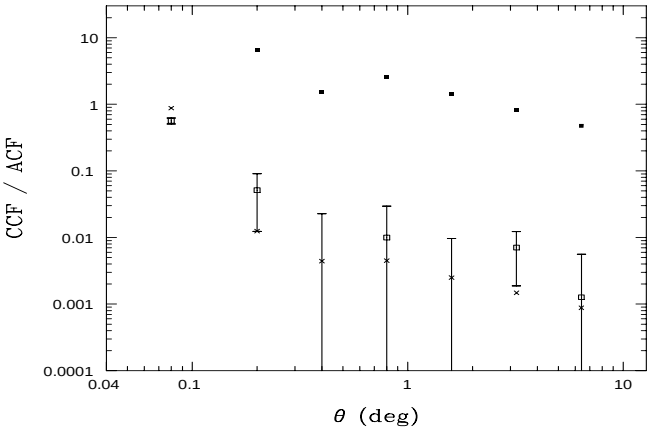

Fig. 3a. Correlation functions for galaxies in sample 1: filled squares – the ACF, open squares and error bars – the CCF of sample 1 and the RASS maps (same as Fig. 2a), crosses – the CCF predicted using correlations between all galaxy samples (see text for details)

Comparison of differences between the simulated and observed CCFs for samples $k = 2-5$ offers a possible explanation of systematic changes of the X-ray–to–optical ratio. The predicted CCF amplitude in sample 3 at $\theta < 0.^\circ5$ is below the observed CCF. A similar effect is present in the sample 2 also at larger separations, although within the error bars. Samples 4 and 5 show near perfect agreement between observations and predictions. These data indicate, albeit at a relatively low significance level, that the total angular extent of X-ray emission associated with galaxies has been underestimated in our calculations in samples 2 and 3, while galaxies in samples 4 and 5 are more distant and their sizes are below the pixel size. To check quantitatively this effect, we have recalculated the X-ray–to–optical ratio and the relative galaxy contribution C_k to the XRB using the first three points instead of two of the ACFs and CCFs, e.g. the correlation functions have been averaged over $\theta < 30'$ rather than $18'$ and the calculations described in Sect. 5 have been repeated. One could expect that this change of the angular separations used in the analysis will not affect results in the samples 4 and 5. In fact, we get now $C_k = 0.31$ and 0.37, respectively. Differences with our previous estimates of 0.33 and 0.38 (Table 4) are clearly within the uncertainties. In the sample 3 we obtain substantially increased X-ray contribution, namely $C_3 = 0.35$, as compared to 0.24 for $\theta < 18'$. A similar but weaker effect is detected in the sample 2: $C_2(< 30') = 0.18$, while $C_2(< 18') = 0.15$. Further increase of separations does not provide more accurate estimates because of the large CCF error bars above $\theta \simeq 1^\circ$. We conclude that variations of C_k could be eliminated assuming that the average X-ray emission by galaxies in sample 3 extends up to $\sim 0.^\circ5$ and even to larger distances in the sample 2. One should note that the accuracy of the CCF measurements is quite low even at these small separations. Inclusion of the $18' < \theta < 30'$ point into the C_k estimates does not reduce the statistical uncertainties involved in our calculations. It shows only that the data are consistent with the supposition that a substantial fraction of the flux correlated with galaxies originates in extended sources. At the same time, the extended emission can explain the variations of C_k found for $\theta < 18'$ in a natural way.

Uncertainties of the relative contribution to the XRB, C_k are produced by various sources. Both statistical as well as systematic effects are present. Our error estimates of the galaxy–X-ray CCFs shown in the figures provide some insight into the problem. These errors are given as signal–to–noise ratio of the CCF measurements in column 5 of Table 2. Because they are directly related to the number of galaxies involved in the computations, sample 5 exhibits the smallest statistical uncertainties. Two other samples which were effectively used to estimate C_k, viz. samples 3 and 4, suffer from substantially larger uncertainties. Nevertheless, all three samples eventually provided very similar estimates of the total galaxy contribution to the XRB. This conspicuous agreement between three samples shows that our approach constitutes an efficient and coherent method of calculations. We note that three samples of galaxies

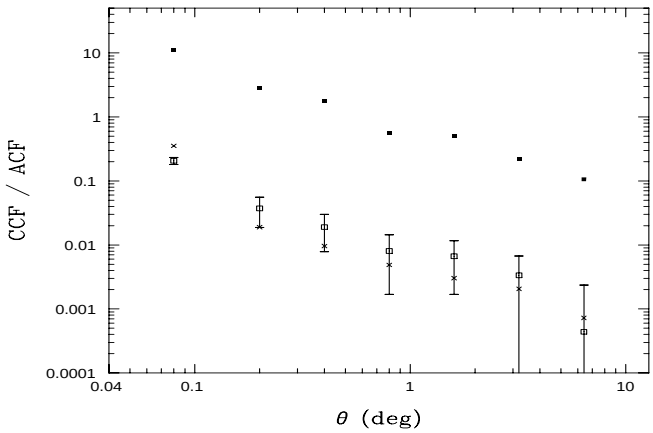

Fig. 3b. Same as Fig. 3a for sample 2

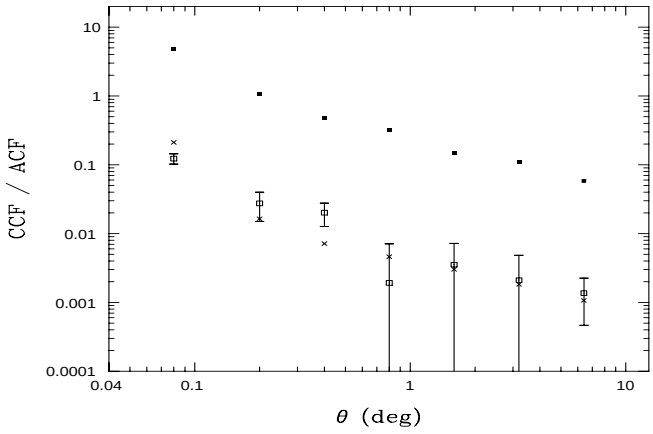

Fig. 3c. Same as Fig. 3a for sample 3

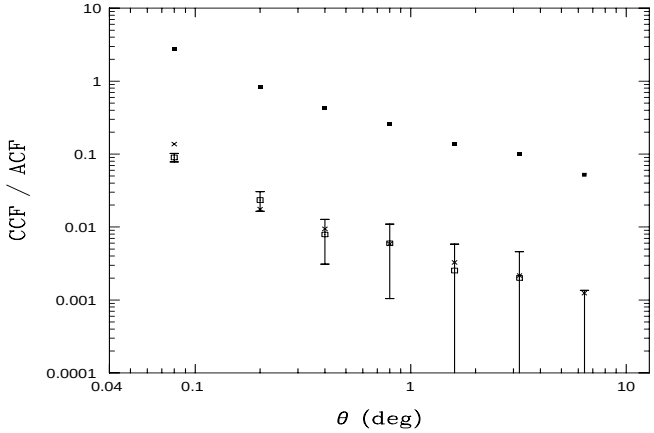

Fig. 3d. Same as Fig. 3a for sample 4

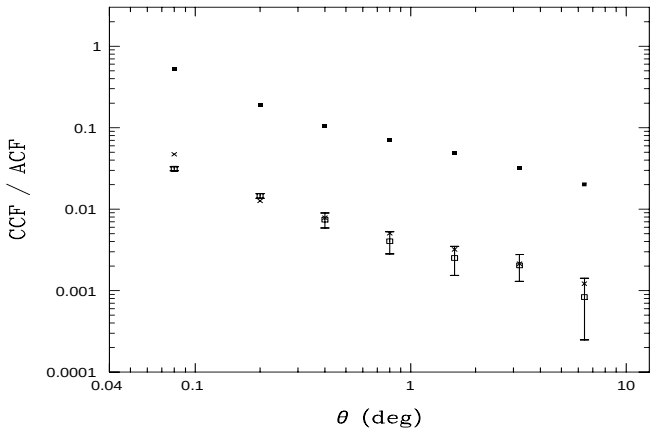

Fig. 3e. Same as Fig. 3a for sample 5

under consideration cover almost 5 magnitudes in the apparent brightness. The range of redshifts is also very wide. The estimated characteristic redshift of the most distant galaxies in the sample 5 exceeds 0.1, while the mean redshift in the sample 3 $\langle z_3 \rangle = 0.018$. The data are quite heterogeneous: sample 3 and 4 come from the PGC while sample 5 is a subset of the SW counts. All these factors as well as the multi–step procedure of the C_k determination make literal assessment of the final errors unreliable. Due to this reason we refrain from formal estimates of the C_k uncertainties. However, the results based on samples 3, 4 and 5 indicate explicitly that the total contribution of X-ray emission associated with the local galaxy population assuming no evolution falls in the range $0.3 \lesssim C_k \lesssim 0.4$.

The large pixel size does not allow for a detailed study of the spatial distribution of the emission. Crude estimates of the magnitudes involved are obtained as follows. Mean galaxy redshifts in samples 2 and 3 are 0.010 and 0.018, respectively. Using the C_k values from Table 4 we find out that roughly half of the X-ray emission by galaxies in sample 2 comes from separations greater than $\sim 18'$ while all the emission in sample 3 comes within $\sim 30'$. Linear sizes corresponding to $\sim 18'$ at $z = 0.010$ and to $\sim 30'$ at 0.018 are 0.16 Mpc and 0.47 Mpc. Thus, half of the emission comes from regions of radius ~ 0.5 Mpc but well outside the optical extent of galaxies. We would like to stress once more that the exact nature of the extended emission introduced to obtain consistent results on the X-ray luminosity density within our data is not well constrained by the correlation analysis. Our estimate that about half of the emission could come from regions of ~ 1 Mpc size does not imply that each galaxy is surrounded by such emitting region. The extended signal could be generated either by weak sources associated with a large number of individual galaxies or by a small number of stronger sources related to galaxy groups or clusters. Below we consider such two models and confront them with observational constraints.

6.1. Cluster emission

Extended X-ray emission by small clusters and groups of galaxies contained in the galaxy samples used in the present investigation offers a natural explanation for the ~ 1 Mpc size X-ray sources reported above. We note that only Abell clusters have been excluded from the data, while all variety of smaller groups as well as some unspecified number of rich clusters missed by

Abell are still present in our material. Obviously, only a fraction of galaxies belongs to those groups or clusters, but our analysis is unable to distinguish between a large number of weak extended haloes around every galaxy and less numerous but stronger X-ray cluster sources. The possible significance of poor cluster emission for the XRB fluctuations is discussed in some details in Paper I. Using analogous arguments we conclude that small groups of galaxies most probably could provide sufficient X-ray emission to reproduce our detection of extended sources. Accurate data on statistics of groups of galaxies and their X-ray emission are unavailable. However, the relationship between various parameters characterizing clusters, such as space density, surface density of galaxies within a cluster ("richness"), velocity dispersion and X-ray luminosity show sufficient continuity between rich and poor clusters (e.g. Edge & Stewart 1991a, b, Henry & Arnaud 1991, David et al. 1993, Dell'Antonio et al. 1994). Although these data do not provide definitive estimates of the cluster volume emissivity, we assess that the mean emissivity of $\sim 5 \times 10^{38}\,\mathrm{erg\,s^{-1}Mpc^{-1}}$ indicated by our study is consistent with the data in the literature. In particular, it coincides with the luminosity density derived from the luminosity function of the X-ray selected groups of galaxies obtained by Henry et al. (1995). On the other hand, the uncertainties of the extrapolation involved in this estimate are large and we do not claim that the extended emission detected in the present investigation is definitely and completely produced in poor clusters.

One should note that the temperature of thermal emission by poor groups of galaxies rarely exceeds 2 keV (Dell'Antonio et al. 1994). Thus, groups of galaxies typically are detected neither by *HEAO 1* A-2 nor *Ginga* LAC experiments which operate in 2–10 keV and 4–12 keV energy bands, respectively. Assuming a thermal emission model, estimates of the normal galaxy contribution to the XRB above 2 keV by Jahoda et al. (1991), Lahav et al. (1993) and Carrera et al. (1995) should be compared to our calculations which exclude extended sources. Splitting the total density luminosity into extended and "point-like" emission, the contribution of each component to the XRB amounts to $\sim 15\,\%$. In this case, the results obtained by "non-imaging" instruments of roughly 30 % are above our estimates. Taking into account the large uncertainties of all analyses, this difference is probably insignificant.

6.2. Galactic halo

We now discuss a possibility that extended emission is associated with individual galaxies rather than groups of galaxies. First, we note that X-ray halo of ~ 1 Mpc diameter with X-ray luminosity below a few times $10^{40}\,\mathrm{erg\,s^{-1}}$ would escape detection as individual source even in extremely deep X-ray exposures. This is because the surface brightness of such extended source does not exceed one per cent of the average XRB intensity and such weak signal falls below the sensitivity limit in virtually all X-ray experiments. Obviously, a source with these parameters is not recognized as a single object also in the present investigation. The correlations analysis could reveal their existence only if such sources constitute sufficiently numerous class of X-ray objects.

Normal galaxies have soft X-ray luminosities between $\sim 10^{38}$ to $\sim 10^{42}\,\mathrm{erg\,s^{-1}}$ (Fabbiano et al. 1992). Detailed observations reveal often complex X-ray morphology and quite frequently there is no one–to–one match between X-ray and optical features (e.g. Fabbiano 1989, Fabbiano et al. 1992). Although some galaxies including our own seem to be surrounded by hot gas emitting soft X-rays (e.g. Pietsch & Trümper 1993, Pietsch 1993, Snowden et al. 1994a, Ehle et al. 1995), the characteristic size of sources reported in the previous section would represent a new constituent of the galaxy X-ray emission. We consider here two alternative models for this halo. First, galaxies may be surrounded by halos of radius 0.5 Mpc of hot gas which radiates X-rays in thermal bremsstrahlung. The gas temperature is not constrained by the present measurement. One can tentatively assume that $kT \lesssim 2$ keV. In the second model, the emission is produced by a large number of weak sources. The possible nature of these sources is unknown, but low mass X-ray binaries, neutron stars, black holes or subdwarfs are potential candidates. We refer to a paper by Maoz and Grindlay (1995) who investigated the possibility of a halo around our Galaxy built with these objects. They found that all the observational constraints are not violated if the Galaxy – and other spirals – is surrounded by a population of $\approx 10^{8-9}$ X-ray sources with luminosities $\approx 10^{30-31}\,\mathrm{erg\,s^{-1}}$ distributed in a halo with a characteristic radius of ~ 15 kpc. It remains to be seen whether identifications of sources from the deepest *ROSAT* pointings will validate this model or impose observational constrains which force some modifications of its parameters. In the latter case one should examine if this model could still provide possible explanation for the extended emission indicated by the present investigation.

7. Conclusions and some prospects for the future

Measurements of the local X-ray volume emissivity are effectively done using correlations between galaxy distribution and the XRB maps. Assuming that the X-ray and optical emissivities are proportional when averaged over large volume of space, we have been able to estimate total production of soft X-rays per cubic Mpc. Such analysis has been performed using several galaxy samples with well defined apparent magnitude limits. Wide range of magnitudes corresponds to substantially different depths of the galaxy samples. However, because of the broad distribution of galaxy absolute optical luminosities, galaxies of quite different apparent magnitudes are spatially correlated. This leads to significant angular correlations on the celestial sphere between galaxy samples. In the present analysis all these effects have been accounted for.

X-ray emission associated with the local population of galaxies contributes to the fluctuations of the XRB on degree scale. The amplitude of these fluctuations can be estimated using our present assessments of the average X-ray luminosity density related to galaxies and fluctuations of the galaxy distribution. In the next paper of this series we intend to evaluate the magnitude of the galaxy induced XRB fluctuations and relate them to the results of Paper I.

The varying ratio of X-ray–to–optical emissivities with redshift and the angular dependence of auto- and cross-correlations indicate the presence of extended X-ray emission. Because of the poor statistics, the intensity of this diffuse X-ray radiation is not well determined. However, the data is consistent with the conjecture that about half of the luminosity comes from regions outside the optical galaxy image. Such extended sources could be associated with extended emission by hot gas in groups and clusters of galaxies, although neither our estimates nor observational data on X-ray properties of such clusters are sufficiently accurate to make a quantitative comparison. One could expect even greater observational difficulties to verify the "halo around each galaxy" model. If the typical X-ray luminosity of a halo is $\sim 10^{39}\,\mathrm{erg\,s^{-1}}$, its detection as a distinct entity would be practically impossible with the present-day instruments. To distinguish between the two models considered here, one needs extensive statistical data on X-ray properties of groups of galaxies. We expect also that a scrupulous selection of "isolated" and "cluster" galaxies in our samples would help to address this question.

Acknowledgements. The *ROSAT* project has been supported by the Bundesministerium für Bildung, Wissenschaft, Forschung und Technologie (BMBF/DARA) and by the Max-Planck-Society. The Authors thank Dr. M. Kurtz for providing them with the electronic version of the Lick galaxy counts. AMS is grateful to Prof. J. Trümper for his hospitality and financial support. This work has been partially supported by the Polish KBN grants 2 P304 021 06 and 2 P03D 005 10.

References

Andreani, P., Cristiani, S., 1992, ApJ 398, L13
Bower, R. G., Hasinger, G., Castander, F. J., et al., 1996, MNRAS 281, 59
Boyle, B. J., Griffiths, R. E., Shanks, T., Stewart, G. C., Georgantopoulos, I., 1993, MNRAS 260, 49
Briel, U. G., Henry, J. P., 1993, A&A 278, 390
Butcher, H. R., van Breugel, W., Miley, G. K., 1980, ApJ 235, 749
Carrera, F. J., Barcons, X., Butcher, J. A., et al., 1995, MNRAS 275, 22
David, L. P., Slyz, A., Jones, C., et al., 1993, ApJ 412, 479
Dell'Antonio, I. P., Geller, M. J., Fabricant, D. G., 1994, AJ 107, 427
Driver, S. P., Phillipps, S., Davies, J. I., Morgan, I., Disney, M. J., 1994, MNRAS 266, 155
Ebeling, H., 1993, Abell and ACO Clusters of Galaxies in the ROSAT All-Sky X-ray Survey: A Statistical Study. PhD Thesis, Garching, MPE report 250
Ebeling, H., Allen, S. W., Crawford, C. S., et al., 1996, In: Zimmermann, H. U., Trümper, J. (eds.) Röntgenstrahlung from the Universe, Garching, MPE report 263, p. 579
Edge, A. C., Stewart, G. C., Fabian, A. C., Arnaud, K. A., 1990, MNRAS 245, 559
Edge, A. C., Stewart, G. C., 1991a, MNRAS 252, 414
Edge, A. C., Stewart, G. C., 1991b, MNRAS 252, 428
Ehle, M., Pietsch, W., Beck, R., 1995, A&A 295, 289
Elvis, M., Soltan, A., Keel, W. C., 1984, ApJ 283, 479
Eskride, P. B., Fabbiano, G., Kim, D.-W., 1995, ApJS 97, 141
Fabbiano, G., 1989, ARA&A 27, 87
Fabbiano, G., Kim, D.-W., Trinchieri, G., 1992, ApJS 80, 531
Hasinger, G., 1992, *ROSAT* Deep Surveys. In: Brinkmann, W., Trümper, J. (eds.) Proc. MPE Conf., X-ray Emission from Active Galactic Nuclei and the Cosmic X-ray Background. Garching, MPE report 235, p. 321
Hasinger, G., Burg, R., Giacconi, R., et al., 1993, A&A 275, 1 (Erratum: A&A 291, 348)
Henry, J. P., Arnaud, K. A., 1991, ApJ 372, 410
Henry, J. P., Gioia, I. M., Maccacaro, T., et al., 1992, ApJ 386, 408
Henry, J. P., Gioia, I. M., Huchra, J. P., et al., 1995, ApJ 449, 422
Iovino, A., Shaver, P. A., 1988, ApJ 330, L13
Jahoda, K., Lahav, O., Mushotzky, R. F., Boldt, E., 1991, ApJ 378, L37
Jahoda, K., Lahav, O., Mushotzky, R. F., Boldt, E., 1992, ApJ 399, L107
Kruszewski, A., 1988, Acta Astron., 38, 155
Lahav, O., Fabian, A. C., Barcons, X., et al. 1993, Nat 364, 693
Lauberts, A., 1982, The ESO/Uppsala Survey of the ESO(B) Atlas, ESO, Garching
Maccacaro, T., Gioia, I. M., Wolter, A., Zamorani, G., Stocke, J. T., 1988, ApJ 326, 680
Maoz, E., Grindlay, J., 1995, ApJ 444, 183
Miyaji, T., Lahav, O., Jahoda, K., Boldt, E., 1994, ApJ 434, 424
Mo, H. J., Fang, L. Z., 1993, ApJ 410, 493
Nilson, P., 1973, Uppsala General Catalogue of Galaxies, Uppsala Astr. Obs. Ann. Vol. 6
Paturel, G., Fouqué, P., Bottinelli, L., Gouguenheim, L., 1989, A&AS 80, 299
Peebles, P. J. E., 1980, The Large Scale Structure of the Universe. Princeton Univ. Press, Princeton, p. 155
Pfeffermann, E., et al., 1987, In: Koch, E.-E., Schamhl, G. (eds.) Soft X-Ray Optics and Technology (Proc. SPIE 733, 519)
Pietsch, W., 1993, In: Hensler, G., Theis, C., Gallagher, J. (eds.) Panchromatic View of Galaxies, Gif-sur-Yvette Cedex, Edition Frontiers, p. 137
Pietsch, W., Trümper, J., 1993, Adv. Space Res. 13, 171
Roche, N., Shanks, T., Georgantopoulos, I., et al., 1995, MNRAS 273, L15
Schechter, P., 1976, ApJ 203, 297
Seldner, M., Peebles, P. J. E., 1977, ApJ 215, 703
Shane, C. D., Wirtanen, C. A., 1967, Publ. Lick Obs., Vol. XXII–part I
Snowden S. L., Schmitt, J. H. M. M., 1990, Ap&SS 171, 207
Snowden, S. L., Hasinger, G., Jahoda, K., et al., 1994a, ApJ 430, 601
Snowden, S. L., McCammon, D., Burrows, D., Mendenhall, J. A., 1994b, ApJ 424, 714
Snowden, S. L., Freyberg, M. J., Plucinsky, P. P., et al., 1995, ApJ 454, 643
Sołtan, A., Hasinger, G., 1994, A&A 288, 77
Sołtan, A. M., Hasinger, G., Egger, R., Snowden, S., Trümper, J., 1996, A&A 305, 17 (Paper I)
Treyer, M. A., Lahav, O., 1995, MNRAS submitted, SISSA bulletin board, astro-ph/9509013
Trümper, J., 1983, Adv. Space Res. 4, (4)241
Turner, E. L., Geller, M. J., 1980, ApJ 236, 1
Voges, W., 1992, In: Guyenne, T. D., Hunt, J. J. (eds.) Science with particular emphasis on High-Energy Astrophysics, Proc. of Satellite Symposium 3, Space (Noordwijk: ESA Publication Division), 9

This article was processed by the author using Springer-Verlag LaTeX A&A style file *L-AA* version 3.